*Journal of Neurochemistry*, 2006, **96**, 1531–1539 doi:10.1111/j.1471-4159.2006.03656.x

# Enhancement of nitric oxide production by association of nitric oxide synthase with *N*-methyl-D-aspartate receptors via postsynaptic density 95 in genetically engineered Chinese hamster ovary cells: real-time fluorescence imaging using nitric oxide sensitive dye

Hirotaka Ishii,*,† Keisuke Shibuya,* Yoshihiro Ohta,‡ Hideo Mukai,*,† Shigeo Uchino,§ Norio Takata,*,† John A. Rose* and Suguru Kawato*,†

*Department of Biophysics and Life Sciences, Graduate School of Arts and Sciences, University of Tokyo at Komaba, Tokyo, Japan
†Core Research for Evolutional Science and Technology Project of Japan Science and Technology Agency, Graduate School of Arts and Sciences, University of Tokyo at Komaba, Tokyo, Japan
‡Department of Biotechnology and Life Science, Tokyo University of Agriculture and Technology, Nakacho, Koganei, Tokyo, Japan
§Department of Neurochemistry, National Institute of Neuroscience, Kodaira, Tokyo, Japan

**Abstract**

The current quantitative study demonstrates that the recruitment of neuronal nitric oxide synthase (nNOS) beneath *N*-methyl-D-aspartate (NMDA) receptors, via postsynaptic density 95 (PSD-95) proteins significantly enhances nitric oxide (NO) production. Real-time single-cell fluorescence imaging was applied to measure both NO production and $Ca^{2+}$ influx in Chinese hamster ovary (CHO) cells expressing recombinant NMDA receptors (NMDA-R), nNOS, and PSD-95. We examined the relationship between the rate of NO production and $Ca^{2+}$ influx via NMDA receptors using the NO-reactive fluorescent dye, diaminofluorescein-FM (DAF-FM) and the $Ca^{2+}$-sensitive yellow cameleon 3.1 (YC3.1), conjugated with PSD-95 (PSD-95-YC3.1). The presence of PSD-95 enhanced the rate of NO production by 2.3-fold upon stimulation with 100 μM NMDA in CHO1(+) cells (expressing NMDA-R, nNOS and PSD-95) when compared with CHO1(–) cells (expressing NMDA-R and nNOS lacking PSD-95). The presence of nNOS inhibitor or NMDA-R blocker almost completely suppressed this NMDA-stimulated NO production. The $Ca^{2+}$ concentration beneath the NMDA-R, $[Ca^{2+}]_{NR}$, was determined to be 5.4 μM by stimulating CHO2 cells (expressing NMDA-R and PSD-95-YC3.1) with 100 μM NMDA. By completely permealizing CHO1 cells with ionomycin, a general relationship curve of the rate of NO production versus the $Ca^{2+}$ concentration around nNOS, $[Ca^{2+}]_{NOS}$, was obtained over the wide range of $[Ca^{2+}]_{NOS}$. This sigmoidal curve had an $EC_{50}$ of approximately 1.2 μM of $[Ca^{2+}]_{NOS}$, implying that $[Ca^{2+}]_{NR} = 5.4$ μM can activate nNOS effectively.

**Keywords:** nitric oxide, neuronal nitric oxide synthase, postsynaptic density 95, diaminofluoroscein, *N*-methyl-D-aspartate receptor.

*J. Neurochem.* (2006) **96**, 1531–1539.

Received August 3, 2005; revised manuscript received October 15, 2005; accepted November 14, 2005.

Address correspondence and reprint requests to Suguru Kawato, Department of Biophysics and Life Sciences and Core Research for Evolutional Science and Technology Project of Japan Science and Technology Agency, Graduate School of Arts and Sciences, The University of Tokyo at Komaba, Tokyo 153–8902, Japan. E-mail: kawato@phys.c.u-tokyo.ac.jp

*Abbreviations used*: CHO cells, Chinese hamster ovary cells; DAF-FM, diaminofluorescein-fluorometry; ECFP, enhanced cyan fluorescent protein; eNOS, endothelial nitric oxide synthase; EYFP, enhanced yellow fluorescent protein; FI, fluorescence intensity; Fura-2/AM, Fura-2 acetoxymethylester; L-NMMA, $N^{\omega}$-monomethyl-L-arginine; LTP, long-term potentiation; NMDA, *N*-methyl-D-aspartate; NMDA-R, *N*-methyl-D-aspartate receptor; nNOS, neuronal nitric oxide synthase; NO, nitric oxide; NOS, nitric oxide synthase; PDZ, PSD-95/Dlg/ZO-1; PSD-95, postsynaptic density 95; YC3.1, yellow cameleon 3.1.

 

Nitric oxide (NO), which is formed by NO synthase (NOS) (Andrew and Mayer 1999), acts as an intercellular and intracellular messenger (Yun *et al*. 1996). In the central nervous system, NO may act as a retrograde messenger between pre- and postsynapses (Yun *et al*. 1996; Hawkins *et al*. 1998) and plays an important role in the induction of long-term potentiation (LTP), for example, in the hippocampus (Hawkins *et al*. 1998; Prast and Philippu 2001). Both the neuronal form of NOS (nNOS) and endothelial NOS (eNOS) are present in principal neurons in the hippocampus (Endoh *et al*. 1994; Iwase *et al*. 1998; Takata *et al*. 2002). Mice lacking both nNOS and eNOS have demonstrated reduced LTP (150%), compared to wild-type LTP (200%) (Son *et al*. 1996). In addition, the application of NOS inhibitors is reported to suppress LTP induction (Doyle *et al*. 1996).

In postsynapses, nNOS is suggested to associate with *N*-methyl-D-aspartate (NMDA) receptors (NMDA-R) via the scaffold protein, postsynaptic density 95 (PSD-95) (Christopherson *et al*. 1999; Valtschanoff and Weinberg 2001), which contains three PSD-95/Dlg/ZO-1 (PDZ) domains and is expressed abundantly in the postsynaptic density. PSD-95 is reported to interact with both nNOS and NMDA receptors via the PDZ domains (Kornau *et al*. 1995; Brenman *et al*. 1996; Niethammer *et al*. 1996; Sattler *et al*. 1999), resulting in the co-localization of nNOS and NMDA receptors. Because nNOS is a $Ca^{2+}$/calmodulin-dependent enzyme (Stuehr 1997), its NO production is likely to be regulated by the influx of $Ca^{2+}$ through NMDA receptors (Christopherson *et al*. 1999; Sattler *et al*. 1999). The specific relationship between NO production and $Ca^{2+}$ influx, however, has yet to be subjected to a detailed investigation.

nNOS in the hippocampus is activated by a calcium influx through NMDA receptors (Garthwaite *et al*. 1988; Bredt and Snyder 1990; Takata *et al*. 2005). However, nNOS is not efficiently stimulated by activation of non-NMDA receptors that also induce a calcium influx (Kiedrowski *et al*. 1992). nNOS might be effectively activated only in the vicinity of NMDA-R, due to the high local $Ca^{2+}$ concentration upon $Ca^{2+}$ influx. This idea is supported by the observation that nNOS is associated with NMDA-R via PSD-95 using immunoprecipitation or immunogold electronmicroscopy (Christopherson *et al*. 1999; Valtschanoff and Weinberg 2001). It is, however, unclear as to which magnitude the association of nNOS with NMDA-R enhances nNOS activity.

Digital fluorescence imaging using an NO-reactive fluorescent dye is a powerful method to investigate real-time, single cell NO production (Kojima *et al*. 1998; Kojima *et al*. 1999), which is not possible via conventional procedures such as NO electrodes, citrulline assay, or electron spin resonance analysis. The single cell imaging of NO and $Ca^{2+}$ is of crucial importance to elucidating the quantitative dependency of NO production on $Ca^{2+}$ concentration. Although the $Ca^{2+}$ concentration in the vicinity of nNOS is essentially important, it has not yet been determined, due to the difficulty of localizing a $Ca^{2+}$ indicator near the NMDA-R + nNOS complex, beneath the membrane. Another difficulty is that the $Ca^{2+}$ concentration in the vicinity of the NMDA-R + nNOS complex may be at a very high level, which is above the sensitivity limits of conventional $Ca^{2+}$ indicators, such as Fura-2.

The current study was designed to determine quantitatively the extent to which the rate of NO synthesis may be enhanced by complex formation of nNOS with NMDA-R via PSD-95. The precise $Ca^{2+}$ concentration in the vicinity of the NMDA-R + nNOS complex was measured via PSD-95 conjugated yellow cameleon, whose $Ca^{2+}$ sensitivity was optimal between 1 and 10 μM. The rate of NO production was measured for selected Chinese hamster ovary (CHO1) cells which expressed protein complexes of NMDA-R + nNOS + PSD-95.

## Materials and methods

### Chemicals

MK-801 was purchased from Sigma (St Louis, MO, USA). NMDA was purchased from BioMol (Pennsylvania, USA). $N^{\omega}$-monomethyl-L-arginine (L-NMMA) was purchased from Wako Pure Chemical (Japan). Fura-2 acetoxymethylester (Fura-2/AM) was purchased from Dojindo (Kumamoto, Japan). The diacetate derivative of DAF-FM was purchased from Daiichi Chemicals (Tokyo, Japan). All other reagents were of the highest grade commercially available.

### Stable transfectant Chinese hamster ovary cells with *N*-methyl-D-aspartate receptors

A CHO line stably transfected with cDNA of NMDA receptors has been described in detail elsewhere (Uchino *et al*. 1997). Briefly, these cells are stably transfected with a plasmid vector containing the cDNA for an NMDA receptor subunit, combined with a *Drosophila* heat shock promoter. GluRε1 (NR2A) subunit cDNA (3.2 kb *Apa*I fragment, nucleotide residues −124 to 3029 from pBKSAζ1) and GluRζ1 (NR1) subunit cDNA (4.4 kb *Nco*I–*Xba*I fragment, nucleotide residues −66–4329 from pSPGRε1) were used. The CHO cells expressing NMDA receptors were routinely cultured in eRDF-1 medium (1 : 1 : 2 mixture medium of Dulbecco's modified Eagle's medium, Ham's Nutrient Mixture F-12 and RPMI1640, without L-gultamate, glycine, and L-aspartate; Kyokuto Pharmaceuticals Tokyo, Japan) supplemented with 10% fetal bovine serum (LifeTech Oriental Tokyo, Japan), 400 μg/mL geneticin (Sigma), 2 μg/mL blasticidin S hydrochloride (Kaken Pharmaceuticals Tokyo, Japan), 10 μg/mL puromycin (Sigma), and 200 μM 2-amino-5-phosphonopentanoic acid (APV, a specific competitive antagonist of the NMDA receptor, from Sigma) in a humidified atmosphere containing 5% $CO_2$.

It should be noted that NMDA receptors were expressed using heatshock procedures by placing cells for 2 h in a $CO_2$ incubator, maintained at 43°C and 5% $CO_2$. Measurements of NO or $Ca^{2+}$ were carried out from 9 to 16 h after the heatshock activation.

 

### Stable expression of neuronal nitric oxide synthase in Chinese hamster ovary (CHO1) cells

Wild type, full-length nNOS cDNA (kindly donated from Dr Kominami) was subcloned into the multiple cloning site (*Xho*I and *Xba*I) of the vector, pcDNA3.1/Hygro(+) (Invitrogen, Carlsbad, CA, USA). For expression of nNOS in CHO cells (stable transfectant CHO cells with NMDA receptors), CHO cells were stably transfected with the vector containing nNOS cDNA, via a lipofection method using PolyFect (Qiagen, Hilden, Germany). Cells stably expressing nNOS (i.e. CHO1) were cultured in a medium containing 400 μg/mL of hygromicin B. Resistant colonies were trypsinized and sampled carefully using cloning rings. Isolated cells were diluted to single cells in culturing medium and plated for cloning. Several consecutive rounds of cloning were repeated. Established clones were stored in liquid $N_2$ prior to experimental usage.

### Analysis of neuronal nitric oxide synthase expression

The expression of nNOS was confirmed by RT–PCR. Total RNAs were extracted from stably transfected CHO cells using ISOGEN (AGPC reagent, Nippongene, Tokyo, Japan). Total RNAs were treated with RNase-free DNase I (TaKaRa Bio., Shiga, Japan) and purified total RNAs were quantitated on the basis of absorbance at 260 nm. Total RNAs were reverse-transcribed using the T-primed first strand cDNA synthesis kit (Invitrogen). cDNA corresponding to 50 ng of total RNA was subjected to RT–PCR analysis. Specific primer pairs designed are as follows: 5′-AGAGTGACAAGGT-GACCATCG-3′ (forward), 5′-GACTTAGGGCTTTGCAGGTTT-3′ (reverse) for nNOS; and 5′-TTGTAACCAACTGGGACGATATGG-3′ (forward), 5′-GATCTTGATCTTCATGGTGCTAGG-3′ (reverse) for β-actin. Samples were PCR amplified for 32 and 28 cycles for nNOS and β-actin, respectively. Specific conditions were as follows. An initial denaturation step was carried out at 94°C for 2 min. This was followed by 32 or 28 cycles of: (i) a 94°C denaturation step (30 s), (ii) a 59°C annealing step (20 s, for both nNOS and β-actin), and (iii) a 72°C extension step (90 s for nNOS and 30 s for β-actin). PCR products were cloned into pGEM-T-Easy vector (Promega, Madison, WI, USA) and sequenced.

The functional expression of nNOS was next observed via NADPH-diaphorase activity in transfected cells. Cells were fixed with 0.5% formaldehyde for 5 min at 37°C and rinsed with phosphate-buffered saline. Diaphorase assay solution (0.05% Triton X-100, 1 mg/mL β-NADPH, 0.25 mg/mL nitro blue tetrazolium in 0.1 M phosphate buffer at pH 7.4) was then added and incubated for 30 min at 37°C. The reaction was terminated via double washing out of the solution. Precipitation of the formazan formed in the cells was verified using a Nikon TMD-300 microscope (Nikon, Tokyo, Japan).

### Transient infection of postsynaptic density 95 to Chinese hamster ovary (CHO1) cells stably transfected with neuronal nitric oxide synthase and *N*-methyl-D-aspartate receptors

In CHO1 cells (expressing NMDA and nNOS), the transient expression of PSD-95 was performed by incorporating cDNA (a generous gift from Dr Lee) into the cloning site (*Eco*RV) of the vector pcDNA3.1/Hygro(+) (Invitrogen) using Ligation Kit Version 2 (TaKaRa Bio.). For the measurements of $Ca^{2+}$ beneath NMDA receptors ($[Ca^{2+}]_{NR}$) in CHO2 cells (expressing NMDA-R and PSD-95-YC3.1), the fusion protein of PSD-95 with YC3.1 (a special type of yellow cameleon) was used (PSD-95-YC3.1). For this, PSD-95 cDNA was fused with YC3.1 cDNA (kindly obtained from Dr Atsushi Miyawaki, Miyawaki *et al*. 1999) using Ligation Kit Version 2 (TaKaRa Bio.). The fused cDNA was incorporated into the cloning site (*Hin*dIII and *Eco*RI) of the vector pcDNA3. These constructed plasmids were confirmed by sequencing. PSD-95 or PSD-95-YC3.1 was expressed in CHO cells with a lipofection method, using PolyFect (Qiagen). Control CHO cells without PSD-95 vector incorporation (but with stably expressed nNOS) were indicated as CHO3 cells. Note that CHO3 cells were infected with YC3.1.

### Immunocytochemistry of neuronal nitric oxide synthase and postsynaptic density 95 in Chinese hamster ovary cells

Expression of nNOS and PSD-95 in CHO cells was confirmed by immunocytochemistry. For this purpose, CHO cells were cultured on glass coverslips in eRDF-1 medium. Two days after plating, the cells on the glass coverslips were rinsed with phosphate-buffered saline, fixed with 4% paraformaldehyde in phosphate-buffered saline for 20 min, at room temperature, and again rinsed with phosphate-buffered saline. The cultures were incubated for 12 h at room temperature with either primary monoclonal anti-nNOS antibody (Sigma) at 1/100 dilution, or primary monoclonal PSD-95 antibodies at 1/250 dilution (Sigma) in a 0.5% Block Ace (a skim milk-based blocking reagent, Dainihon Pharmaceuticals, Osaka, Japan). Thereafter, cells were incubated for 1 h with biotinylated anti-mouse IgG secondary antibody (1/200, Vector Laboratories, Burlingame, CA, USA), then incubated in streptavidin-Oregon Green 488 (1/1000, Molecular Probes, Eugene, OR, USA) for 1 h. Fluorescence images were analyzed with a cooled CCD Camera (ORCA-ER, Hamamatsu Photonics, Shizuoka, Japan).

### Cell loading with fluorescence indicators

Cells were loaded for 60 min at 37°C, with either 10 μM DAF-FM or 5 μM Fura-2/AM (from a 1 mM stock solution in dimethyl sulfoxide, Dojindo) in the presence of 0.02% Cremophor EL (Sigma) in 1 mL of BSS buffer ($Mg^{2+}$-free 10 mM HEPES buffer, pH 7.3, containing 130 mM NaCl, 5.4 mM KCl, 2.0 mM $CaCl_2$, 5.5 mM glucose, and 10 μM glycine). The maximum concentration of the dimethyl sulfoxide in the observation medium was less than 0.1%, and no side-effect was observed at this concentration.

### Fluorescence imaging and analysis

The digital fluorescence microscope employed consisted of an inverted microscope (Nikon TMD-300) equipped with a high sensitivity cooled CCD camera (Hamamatsu Photonics C2400–77ER). Glass-bottom dishes were mounted on a microscope equipped with a temperature chamber that maintained an air atmosphere of 37°C. Prior to fluorescence observation, cells were rinsed with BSS.

To determine the $Ca^{2+}$ concentration on the cytosolic side of NMDA-R ($[Ca^{2+}]_{NR}$), the fluorescence energy transfer between ECFP (enhanced cyan fluorescent protein) and EYFP (enhanced yellow fluorescent protein) components of PSD-95-YC3.1 was measured by monitoring the ratio of the fluorescence intensities at 535 nm to 480 nm ($F_{535}/F_{480}$) (Miyawaki *et al*. 1999. ECFP was

excited at 430 nm. The fluorescence of ECFP and EYFP was detected at 480 nm and 535 nm, respectively, using a DM455 dichroic mirror. For both proteins, the exposure time was 1 s. The fluorescence at each wavelength was measured once before and once after NMDA stimulation. In many cases, $[Ca^{2+}]_{NR}$ was analyzed at the cellular circumference, because the signal-to-noise ratio of $F_{535}/F_{480}$ was much higher at the circumference than at the central part of the cells. Around the center of the cells we collected mixed fluorescence signals from the cytosol and the membranes. For imaging of fluorescence signals of only membrane-associated probes, we needed to select the circumference of the cell. For calculation, we chose the pixels along the circumference of the cell and averaged the integrated fluorescence intensity by dividing with the total pixel area.

To determine the cytosolic $Ca^{2+}$ concentration ($[Ca^{2+}]_c$), fura-2 fluorescence above 520 nm was measured using a DM400 dichroic mirror and a BA520 emission filter. The excitation wavelength was alternated between 340 nm and 380 nm with a rotary excitation wheel, in the following time sequence: 340 nm exposure for 0.5 s; 380 nm exposure for 0.5 s; closure for 4 s; 340 nm exposure for 0.5 s; 380 nm exposure for 0.5 s, etc. The time resolution of measurement was 5 s. Measurements of intracellular $Ca^{2+}$ concentration are expressed in terms of $F_{340}/F_{380}$, which denotes the ratio of the fura-2 fluorescence intensity at 340 nm excitation ($F_{340}$) to that at 380 nm excitation ($F_{380}$).

To measure the rate of NO production, DAF-FM was excited at 480 nm with an IF excitation filter. The fluorescence above 520 nm was measured with a DM510 dichroic mirror and a BA520 emission filter. To reduce photobleaching of DAF-FM during long-time measurements, fluorescence images were recorded for the first second of each 10-s interval, using a rotary excitation wheel and the following time sequence: 480 nm exposure for 0.2 s; closure for 9.8 s. The time resolution of measurements was 10 s. Images were analyzed using AquaCosmos software (Hamamatsu Photonics). Acquired images were stored on hard disk, using a 512 × 512 pixel resolution, at a 12 bit depth. The fluoresence intensity (FI) of each cell was calculated in a 10 × 10 pixel region marked within a single cell. The rate of NO production [FI/4 min] was calculated by monitoring the increase in the fluorescence of DAF-FM for 4 min after NMDA application.

### Data analysis

To determine $[Ca^{2+}]_{NR}$ and $[Ca^{2+}]_c$, the $F_{535}/F_{480}$ ratio of YC3.1 and the $F_{340}/F_{380}$ ratio of Fura-2 were calibrated into intracellular free $Ca^{2+}$ concentration by permeating the cell membranes with ionomycin, a $Ca^{2+}$ ionophore. To determine the intracellular concentration of NO, DAF-FM fluorescence was calibrated into the concentration of (+/–)-(E)-4-ethyl-2-[(E)-hydroxyimino]-5-nitro-3-hexenamide (NOR3), a NO donor. Data was collected from at least three different dishes. Student's *t*-test (for two groups) and ANOVA, followed by the Tukey multiple comparison test (for three or more groups) were used to determine the statistical significance of any difference.

$Ca^{2+}$ titrations were performed by reciprocal dilution with $Ca^{2+}$-free and $Ca^{2+}$-saturated buffers. *In situ* calibration for $[Ca^{2+}]$ used the equation (Williams *et al*. 1985; Williams and Fay 1990), $[Ca^{2+}] = K'_d[(R - R_{min})/(R_{max} - R)]^{1/n}$, where $K'_d$ denotes the apparent dissociation constant corresponding to the $Ca^{2+}$ concentration at which $R$ is midway between $R_{max}$ and $R_{min}$, and $n$ is the Hill coefficient.

## Results

### Co-expression of postsynaptic density 95, nitric oxide synthase, and *N*-methyl-D-aspartate receptors in Chinese hamster ovary (CHO1) cells

To prepare CHO1(+) cells (expressing NMDA-R, PSD-95 and nNOS), PSD-95 was transiently expressed in CHO1 cells which had been stably transfected with nNOS, after which NMDA receptors were expressed using heat shock procedures. The expression and localization of PSD-95 protein in CHO1 cells was investigated via immunocytochemistry, using anti-PSD-95 IgG. PSD-95 was observed on the cytosolic face of the plasma membrane, in approximately 21% of the CHO1 cells (Fig. 1a). Note that the expression of nNOS mRNA was confirmed by RT–PCR in CHO1 cells stably transfected with nNOS (Fig. 1b).

The localization of nNOS protein was examined with immunofluorescence staining using anti-nNOS IgG. In CHO1(+) cells expressing PSD-95, nNOS was expressed predominantly at the plasma membrane, and also to a small extent in the cytosol (Fig. 1c). In contrast, nNOS was exclusively localized in the cytosol of CHO1(–) cells lacking PSD-95 expression (Fig. 1d). These results imply that nNOS is efficiently conjugated to NMDA receptors via PSD-95, resulting in localization at the plasma membrane. Note that the sensitivity of fluorescence detection was different between Figs 1(c) and (d). The sensitivity in Fig. 1(d) was higher in order to observe even a weak fluorescence signal from non-aggregated nNOS. The total fluorescence intensity within CHO cells was approximately the same between Figs 1(c) and (d) when the sensitivity was the same, because both CHO1(+) and CHO1(–) cells were made from the same CHO1 cells expressing nNOS stably. We also examined nNOS expression in CHO cells by measuring diaphorase activity. A significant formazan formation was predominantly observed in nearly all CHO1(+) and CHO1(–) cells (data not shown).

### Determination of $Ca^{2+}$ concentration

Upon stimulation with NMDA, a $Ca^{2+}$ influx stimulates nNOS complexed with NMDA receptors. Accordingly, measurement of the $Ca^{2+}$ concentration on the cytosolic side of NMDA-R ($[Ca^{2+}]_{NR}$) is necessary, because $[Ca^{2+}]_{NR}$ is probably much higher than the bulk cytosolic concentration of $Ca^{2+}$ ($[Ca^{2+}]_c$), upon $Ca^{2+}$ entry. To determine $[Ca^{2+}]_{NR}$, we expressed the fusion protein of yellow cameleon 3.1 (YC3.1) with PSD-95 (PSD-95-YC3.1) in CHO2 cells (NMDA-R + PSD-95-YC3.1). Localization of PSD-95-YC3.1 was observed on

 

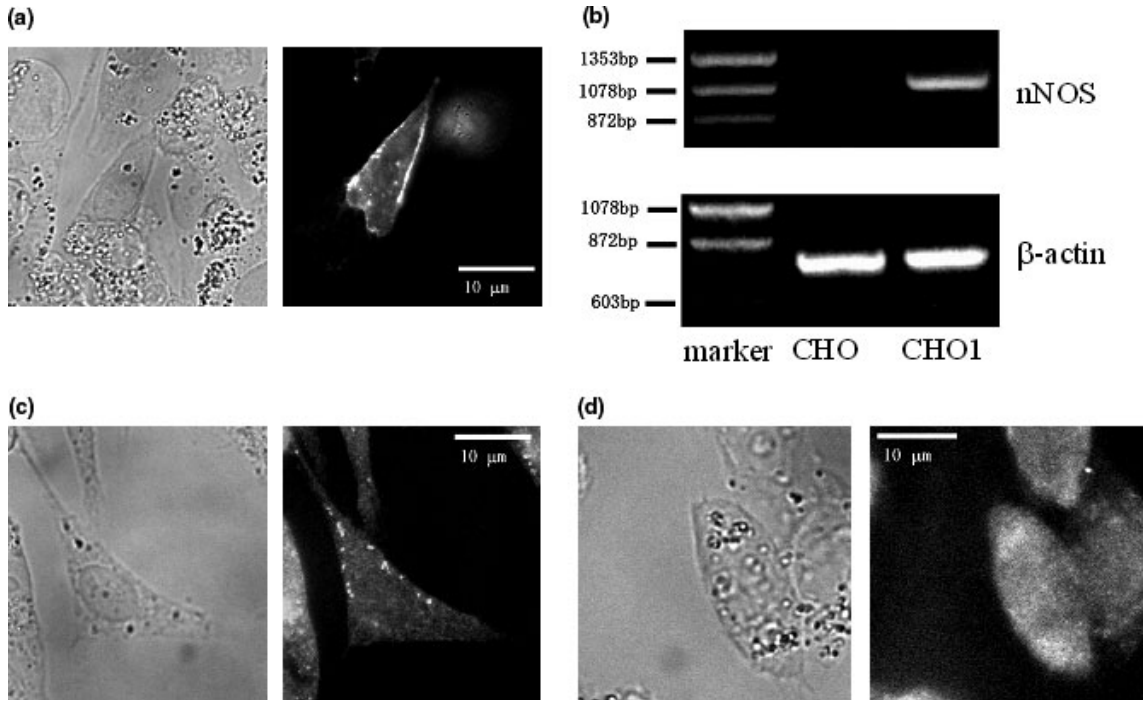


**Fig. 1** Analysis of expression of postsynaptic density 95 (PSD-95) and neuronal nitric oxide synthase (nNOS) in CHO1 cells in which *N*-methyl-D-aspartate receptors (NMDA-R) and nNOS are stably expressed. (a) Localization of PSD-95 at the plasma membrane of CHO1(+). Left panel, bright field image of cells; right panel, staining of cells with anti-PSD-95 IgG in the same field as the left image. (b) RT–PCR analysis of nNOS mRNA. The RT–PCR products for nNOS mRNAs (50 ng each) were electrophoresed on a 1.5% agarose gel, and visualized with ethidium bromide. Upper left lane, markers; upper middle (CHO), control CHO cells expressing only NMDA receptors; upper right lane (CHO1), CHO1 cells which consist of both PSD-95-expressed CHO1(+) and PSD-95-non-expressed CHO1(–) cells. As an internal control, the ethidium bromide staining of β-actin mRNAs is shown in the lower panel (middle and right). (c) Immunocytochemical staining of nNOS in CHO1(+) cells expressing both NMDA-R and PSD-95. Left panel, bright field image of cells; right panel, staining of cells with anti-nNOS IgG in the same field as the left image. (d) Immunocytochemical staining of nNOS in CHO3 cells not transfected by PSD-95 vector. Left panel, bright field image of cells; right panel, staining of cells with anti-nNOS IgG in the same field as the left image. Each analysis was repeated at least three times, with essentially identical results. Scale bar, 10 μm in (a), (c), and (d).

the cytosolic face of the plasma membrane, as determined via cameleon fluorescence (Fig. 2a). When expressed alone, YC3.1 was observed exclusively in the cytosol (Fig. 2b). We measured $[Ca^{2+}]_{NR}$ by monitoring the ratio of the fluorescence intensities at 535 nm and 480 nm ($F_{535}/F_{480}$) of PSD-95-YC3.1 in CHO2 cells. Application of 100 μM NMDA increased the $F_{535}/F_{480}$ from 1.31 to 1.57 (Fig. 2c), indicating an increase in $[Ca^{2+}]_{NR}$ to 5.4 μM. When 30 μM NMDA was applied, $F_{535}/F_{480}$ was observed to increase to 1.47 (in $[Ca^{2+}]_{NR}$ to 2.4 μM). This indicates that NMDA induces the influx of $Ca^{2+}$ in a dose-dependent manner. When free YC3.1 was expressed (i.e. without conjugation with PDS-95), $F_{535}/F_{480}$ did not increase upon application of 100 μM NMDA, indicating that $[Ca^{2+}]_c$ in the cells did not increase to the level of cameleon's $Ca^{2+}$ sensitivity, as $F_{535}/F_{480}$ does not change when the $Ca^{2+}$ concentration is less than 1 μM (which has an $EC_{50}$ of 1 μM). Fura-2 was therefore used to measure small increases in $[Ca^{2+}]_c$. Upon application of 100 μM NMDA, the fluorescence ratio ($F_{340}/F_{380}$) increased from 1.05 to 1.41, which corresponds to an increase in $[Ca^{2+}]_c$ from 120 nM to 587 nM. Removal of extracellular $Ca^{2+}$, or addition of the NMDA receptor inhibitor, MK-801, induced no elevation in either $[Ca^{2+}]_{NR}$ or $[Ca^{2+}]_c$, indicating that the rise in $[Ca^{2+}]_{NR}$ and $[Ca^{2+}]_c$ attendant upon stimulation with NMDA was due to an influx of $Ca^{2+}$ from the medium to the CHO cells. In addition, the expression of PSD-95 had no effect on $[Ca^{2+}]_c$.

### Effects of postsynaptic density 95 on the nitric oxide production by forming a complex with neuronal nitric oxide synthase and *N*-methyl-D-aspartate receptors

$[Ca^{2+}]_{NR}$ became much higher than $[Ca^{2+}]_c$ upon stimulation with NMDA. Because the activity of nNOS depends on the concentration of $Ca^{2+}$, the activity of nNOS located beneath the plasma membrane is expected to be much higher than that in the cytosol. To test this hypothesis, we compared the rate of NO production in CHO1(+) cells expressing PSD-95 (PSD-95 was present in addition to NMDA-R and nNOS)

 

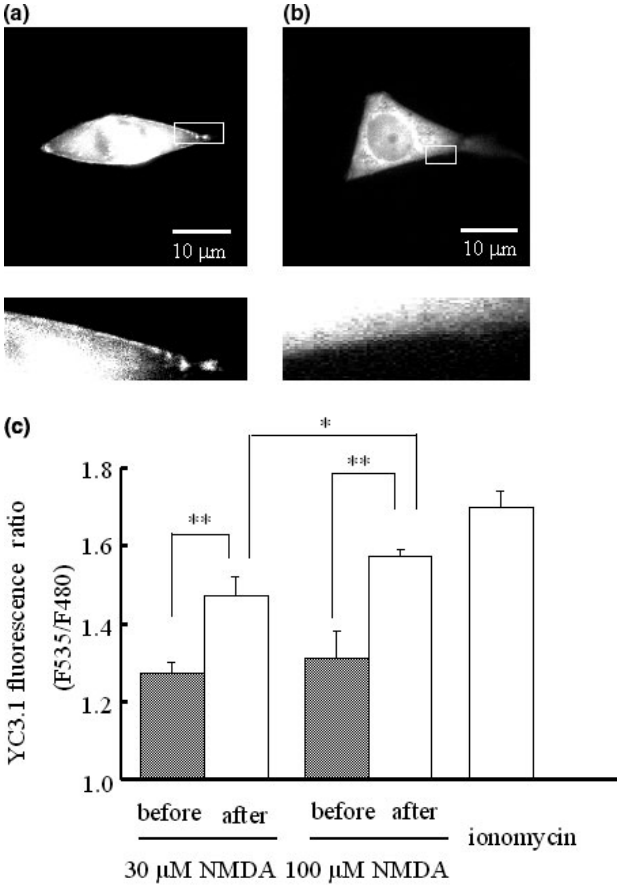


**Fig. 2** $Ca^{2+}$ concentrations beneath the *N*-methyl-D-aspartate (NMDA) receptors, as measured with yellow cameleon 3.1 (YC3.1). (a) Fluorescence image of the fusion protein of YC3.1 with postsynaptic density 95 (PSD-95) in CHO2 cells, 4 min after the application of NMDA. The lower image is the magnified image of the rectangular region in the upper image. (b) Fluorescence image of YC3.1 without PSD-95 in CHO3 cells, 4 min after the application of NMDA. The lower image is the magnified image of the rectangular region. (c) $Ca^{2+}$ concentrations beneath the NMDA receptors. $Ca^{2+}$ concentrations were measured by averaging the fluorescence ratio of YC3.1 ($F_{535}/F_{480}$) along the cellular circumference. The fluorescence ratio was determined before (before) and 4 min after (after) the application of NMDA. Values of columns in (c) represent the mean ± SEM obtained for 31–42 cells in five independent experiments for each NMDA applications. The values of $[F_{535}/F_{480}] = 1.47$ and 1.57 correspond to $[Ca^{2+}]_{NR} = 2.4$ and 5.4 μM, respectively. The maximum fluorescence ratio was obtained by the application of 4 μM ionomycin to cells, in the presence of outer $Ca^{2+}$ concentration, $[Ca^{2+}]_{out}$, at 2 mM. Note that the fluorescence ratio was already saturated at $[Ca^{2+}]_{out} = 20$ μM. The significance of the NMDA-induced $Ca^{2+}$ elevation was confirmed using the Student's *t*-test (*$p < 0.05$; **$p < 0.01$). Scale bar, 10 μm in (a) and (b).

with that in CHO1(–) cells not expressing PSD-95 (PSD-95 was absent, NMDA-R and nNOS were expressed). As PSD-95 was expressed in only a subset of the cells, those expressing PSD-95 were identified via immunofluorescence staining after measuring NO production. The rate of NO production [FI/4 min] was measured by monitoring the increase in the fluorescence of DAF-FM over 4 min after NMDA application. Because the reaction of NO with DAF-FM is irreversible, DAF-FM fluorescence intensity remains stable after reaction with NO. The DAF-FM fluorescence intensity is therefore indicative of cumulative NO production at the time of measurement.

Upon application of 100 μM NMDA, the rate of NO production was increased, by approximately 25% in CHO1(+) cells and 11% in CHO1(–) cells. The fluorescence intensity of DAF-FM corresponded to NO concentration of 2.1 μM and 0.6 μM, respectively, at 4 min after the NMDA stimulation (Fig. 3b).

In CHO3 cells (NMDA-R + nNOS without PSD-95) where only cytosolic nNOS was present, 100 μM NMDA stimulation increased the rate of NO production by only approximately 11%. Cytosolic $Ca^{2+}$ concentration increased to 587 nM ($F_{340/380} = 1.41$), as measured with fura-2, upon 100 μM NMDA application.

These results indicate that the presence of PSD-95 significantly enhanced the rate of NO production [FI/4 min] in CHO cells expressing nNOS and NMDA receptor. In addition, the increase in the concentration of applied NMDA from 30 μM to 100 μM enhanced the rate of NO production (Fig. 3c).

It should be noted that 30 μM MK-801 (an NMDA-R blocker), 50 μM L-NMMA (an inhibitor of nNOS), and the absence of extracellular $Ca^{2+}$ almost completely suppressed the rate of NO production [FI/4 min], indicating that nNOS is stimulated by the increase in $Ca^{2+}$ (Fig. 3d).

### $Ca^{2+}$ concentration dependence of nitric oxide production by neuronal nitric oxide synthase in Chinese hamster ovary cells

The relationship between intracellular $Ca^{2+}$ concentration and the rate of NO production was determined in CHO1 cells, rendered $Ca^{2+}$-permeable by the presence of 4 μM ionomycin, by monitoring the fluorescence of DAF-FM. For $Ca^{2+}$ concentrations of the outer medium, $[Ca^{2+}]$ ranging from 20 nM to 2 mM, the rate of NO production was observed to increase sigmoidally with increasing $Ca^{2+}$ concentration, with an $EC_{50}$ of approximately 1.2 μM (Fig. 4). In Fig. 4, the rate of NO production was approximately 28 [FI/4 min] at $[Ca^{2+}] = 5.4$ μM. This is in a good agreement with the relationship obtained from Figs 2(c) and 3(c), in which the rate of NO production was approximately 25 [FI/4 min] (Fig. 3c) at $[Ca^{2+}]_{NR} = 5.4$ μM ($[F_{535}/F_{480}] = 1.57$ (Fig. 2c)). This supports the equal value between extracellular and intracellular concentrations by the presence of 4 μM ionomycin. It should be noted that this relationship shown in Fig. 4 may be applicable to many cell types, because the relationship is independent of the number

 

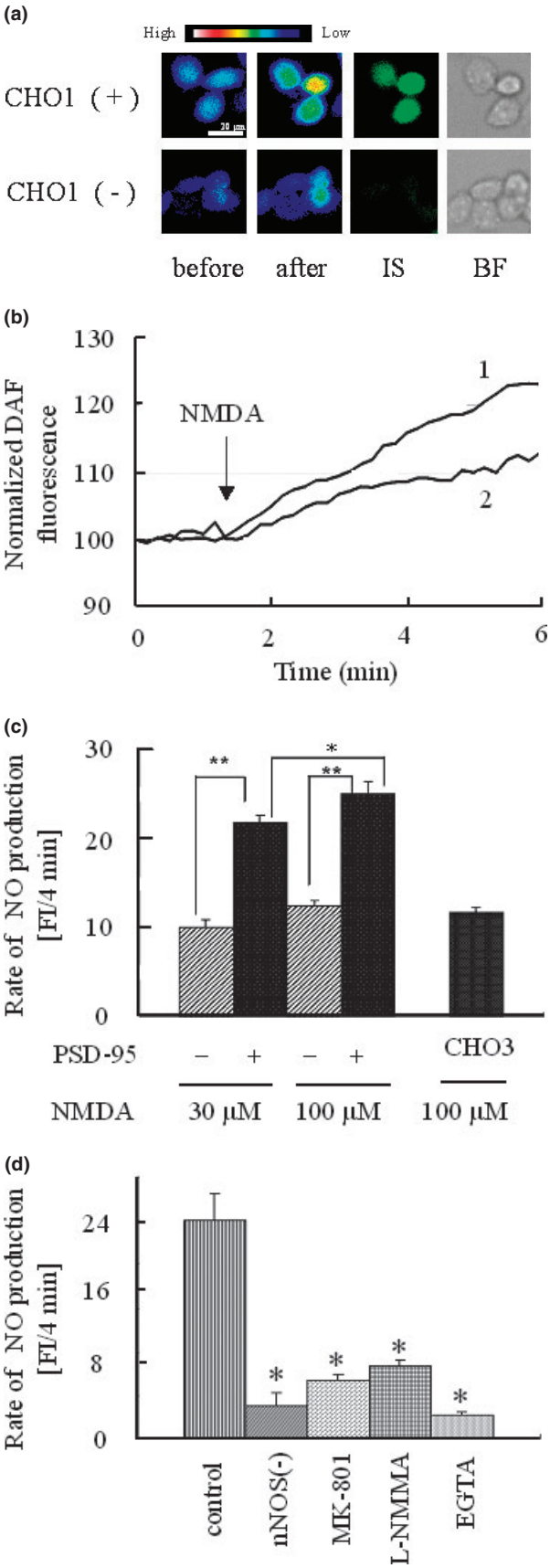


**Fig. 3** Rate of nitric oxide (NO) production upon the application of *N*-methyl-D-aspartate (NMDA). (a) Representative images of diaminofluorescein-FM (DAF-FM) fluorescence in CHO1 cells expressing postsynaptic density 95 (PSD-95) [CHO1(+), top], and in CHO1 without PSD-95 [CHO(–), bottom] in the same dish. The fluorescence images were captured before (before) and 4 min after (after) the application of NMDA. The expression of PSD-95 was confirmed by immunocytochemical staining (IS) with anti-PSD-95 IgG. BF indicates bright field images of cells. These images were chosen from the same culture dish. Essentially identical results were observed from 13 independent experiments. Scale bar, 20 μm. (b) Time course of the representative DAF-FM fluorescence curves in CHO1(+) cells expressing PSD-95 (line 1), and in CHO1(–) without PSD-95 (line 2); the curves were chosen from 68 and 78 data curves, respectively. DAF-FM fluorescence at $t = 0$ (NMDA application) is normalized to 100. (c) Average rate of NO production was illustrated as the rate of DAF-FM fluorescence increase [FI/4 min] from 62 to 81 cells over 4 min after the application of NMDA. PSD-95 – and + indicate the absence [CHO1(–) cells] and presence [CHO1(+) cells] of PSD-95 protein, respectively. CHO3 cells are not infected by PSD-95 plasmid, therefore no PSD-95 was expressed. The applied NMDA amounts (30 μM and 100 μM) are also indicated. Values of columns in (c) represent the mean ± SEM values obtained from 62 to 81 cells in five independent experiments for each NMDA applications. (d) Effect of inhibitors. The average rate of NO production, illustrated as the rate of DAF-FM fluorescence increase [FI/4 min], from 158 to 192 cells over 4 min following stimulation with 100 μM NMDA was measured. Values of columns in (d) represent the mean ± SEM obtained from 158 to 192 cells in eight independent experiments for each NMDA applications. From left to right, control CHO1(+) cells (control), CHO cells without nNOS [nNOS(–)],CHO1(+) cells in the presence of 30 μM MK-801 (MK-801), CHO1(+) cells in the presence of 50 μM $N^{\omega}$-monomethyl-L-arginine (L-NMMA), and CHO1(+) cells in the presence of 1 mM EGTA-$Ca^{2+}$ free buffer (EGTA). Data are expressed in terms of the rate of DAF-FM fluorescence increase (i.e. the rate of NO production) induced by 100 μM NMDA. The significance of the NMDA-induced increase in DAF-FM fluorescence was confirmed using the Student's *t*-test (*$p < 0.05$; **$p < 0.01$).

of PSD-95 or NMDA-R, only dependent on $Ca^{2+}$ concentration at around nNOS.

## Discussion

### Cameleon is useful for measuring high $Ca^{2+}$ concentrations at the cytosolic side of *N*-methyl-D-aspartate receptors and other $Ca^{2+}$ channels

Taking advantage of genetic engineering, the ability to localize cameleon at mitochondria, the endoplasmic reticulum, and the surface of secretory vesicles has enabled the local concentrations of $Ca^{2+}$ to be selectively determined in these regions. In the present study, PSD-95-YC3.1 was localized beneath the NMDA receptors, and the local $Ca^{2+}$ concentration was determined to be $[Ca^{2+}]_{NR} = 5.4$ μM, which is much higher than $[Ca^{2+}]_c = 0.6$ μM, the level observed in the entire cytosol using fura-2, upon NMDA stimulation. This is the first

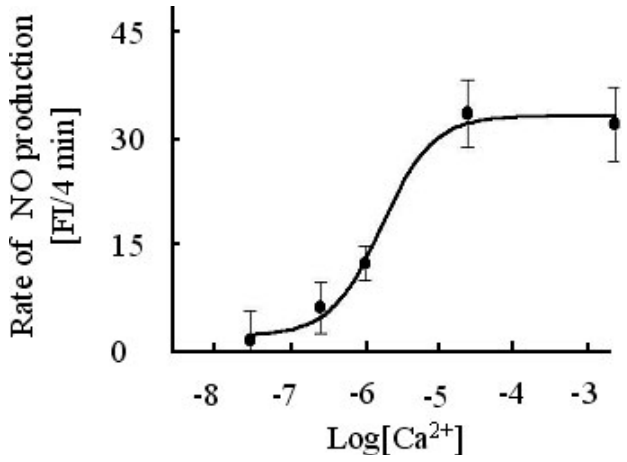


**Fig. 4** Relationship between the rate of nitric oxide (NO) production and intracellular $Ca^{2+}$ concentration. $Ca^{2+}$-dependent activation of neuronal nitric oxide synthase (nNOS) in $Ca^{2+}$-permeable CHO1 cells by the presence of ionomycin. Vertical axis indicates the rate of NO production [FI/4 min], determined from the rate of DAF-FM fluorescence increase over 4 min upon application of 4 μM ionomycin, which was used to make the intracellular $Ca^{2+}$ concentration the same as the $Ca^{2+}$ concentration in the outer medium. Note that the $Ca^{2+}$ concentration within CHO1 cells reached a maximal value within 1 min. Horizontal axis indicates the $Ca^{2+}$ concentration in the outer medium [$Ca^{2+}$]. Each value represents mean ± SEM obtained for 50–65 cells in four independent experiments.

demonstration of the determination of the $Ca^{2+}$ concentration beneath $Ca^{2+}$ channels. We exploited cameleon's low $Ca^{2+}$ sensitivity, as reflected by an $EC_{50}$ of 1.0 μM, for use as a $Ca^{2+}$ indicator on the cytosolic side of membrane receptors, in the vicinity of which the $Ca^{2+}$ concentration may be between 1 and 10 μM. The current results provide a good model for the novel usage of cameleon. It should be noted that it is impossible to accurately measure such a high calcium concentration of $[Ca^{2+}]_{NR} = 5.4$ μM using fura-2, because this level is sufficiently high as to be beyond fura-2's sensitivity. Previously, instead of pin-point detection at $Ca^{2+}$ channels, the local $Ca^{2+}$ concentration beneath the plasma membrane was determined using either FFP-18 (a lipid conjugated dye) (Davies and Hallett 1995; Etter *et al*. 1996), or aequorin fused with SNAP-25 (a lipophilic segment) (Marsault *et al*. 1997). Upon $Ca^{2+}$ entry from the medium, the $Ca^{2+}$ concentration beneath the plasma membrane was measured at 2 μM in smooth muscle cells (Etter *et al*. 1996), 10 μM in smooth muscle cell line A7r5 (Marsault *et al*. 1997), and 30 μM in neutrophils (Davies and Hallett (1995)). Consistent with our present observations, these results demonstrate that the concentration of $Ca^{2+}$ beneath the plasma membrane is much higher than that in the cytosol, upon $Ca^{2+}$ influx. Determination of a $Ca^{2+}$ concentration of 5.4 μM beneath the NMDA-R is essential for a consideration of $Ca^{2+}$-dependent signal cascades in neuronal postsynapses and of synaptic plasticity.

### A high $[Ca^{2+}]_{NR}$ is effective for neuronal nitric oxide synthase activation

In the current study, the rate of NO production was significantly increased by NMDA stimulation only in CHO cells expressing both PSD-95 and NMDA-R (see Fig. 3). The increase in $Ca^{2+}$ concentration, up to $[Ca^{2+}]_{NR} = 5.4$ μM at the probable position of nNOS, was sufficiently high to effectively activate nNOS, as judged by an $EC_{50}$ of 1.2 μM, determined from the sigmoidal relationship between nNOS activity and $Ca^{2+}$ concentration (see Fig. 4). This result indicated the functional coupling of nNOS with NMDA-R, via PSD-95, and is consistent with the observation that the presence of PSD-95 resulted in the localization of nNOS predominantly at the cytosolic face of the plasma membrane (see Fig. 1c). As demonstrated in many reports, PSD-95 functions as a scaffold protein for the association of nNOS with NMDA-R, via PDZ domains (Christopherson *et al*. 1999; Sattler *et al*. 1999).

In the absence of PSD-95, NMDA stimulation resulted in only a weak increase in the rate of NO production (see Fig. 3c). Furthermore, nNOS was distributed over the entire cytosolic space, as judged from the immunostaining of nNOS (Fig. 1d). This small rate of NO production was, therefore, consistent with a weak rise in $[Ca^{2+}]_c$ (to 0.6 μM), which is much lower than the $EC_{50}$ of 1.2 μM, as determined via the sigmoidal relationship between nNOS activity and $Ca^{2+}$ concentration (see Fig. 4).

It has been suggested that nNOS, PSD-95 and NMDA-R form a ternary complex in the postsynaptic density (Christopherson *et al*. 1999). As $[Ca^{2+}]_{NR}$ should become high upon NMDA stimulation, it has also been proposed that nNOS might be effectively activated within the ternary complex upon NMDA stimulation. The aim of the present study is to prove this hypothesis with model cells. Our current results clearly demonstrate that the association of nNOS with NMDA-R via PSD-95 enhances the rate of NO production by 2.3-fold upon NMDA stimulation. Although this enhancement is not very great, this is the first experimental proof of the above hypothesis using cell models. As both nNOS and eNOS are expressed in neurons, it would seem that the contribution of NO synthesized by eNOS should be considered. However, this may not be the case. In hippocampus from mice lacking nNOS, the production of NO was 1.7% of that of the wild type (Son *et al*. 1996), indicating that the majority of the NO in the hippocampus is synthesized by nNOS. Therefore, CHO1 cells expressing nNOS, PSD-95 and NMDA-R used in the present study forms a good model for examining NO synthesis in neurons.

### Others

An advantage of single cell NO/$Ca^{2+}$ imaging is the ability to select, by immunostaining following NO/$Ca^{2+}$ measurements, specific cells expressing either protein complexes consisting of NMDA receptors, PSD-95 and nNOS, or

 

protein complexes consisting of NMDA receptors and PSD-95-YC3.1. This is essential, since in practice only a portion of the CHO cells expressed PSD-95, because PSD-95 was expressed via transient transfection. In order to quantitatively determine the effect of PSD-95 on nNOS, nNOS and NMDA receptors should be stably expressed in all CHO cells used. When transient transfection procedures were employed for nNOS expression, an extremely small population (< 5%) of CHO cells expressed both nNOS and PSD-95, which presented a serious difficulty for the investigation of the effect of PSD-95 on nNOS activity, even via single cell NO/$Ca^{2+}$ imaging. The current results may serve to establish a good model system for understanding NO production at postsynapses of neurons, by nNOS complexed with NMDA receptors. Determination of a $Ca^{2+}$ concentration of 5.4 μM beneath the NMDA-R is essential for consideration of $Ca^{2+}$-dependent signal cascades in postsynapses of neurons.

## Acknowledgements

The authors are very grateful to Drs Hirotatsu Kojima and Tetsuo Nagano at the University of Tokyo for helpful advice and discussions on DAF-FM. We are also grateful to Dr Atsushi Miyawaki at RIKEN Brain Science Institute for the generous gift of yellow cameleon 3.1. Dr Shiro Kominami at Hiroshima University is acknowledged for the generous gift of purified nNOS and nNOS cDNA. Dr Yun-Sik Lee is acknowledged for the generous gift of PSD-95 cDNA.

## References

Andrew P. J. and Mayer B. (1999) Enzymatic function of nitric oxide synthases. *Cardiovasc. Res.* **43**, 521–531.

Bredt D. and Snyder S. (1990) Isolation of nitric oxide synthetase, a calmodulin-requiring enzyme. *Proc. Natl Acad. Sci. USA* **87**, 682–685.

Brenman J. E., Chao D. S., Gee S. H. *et al.* (1996) Interaction of nitric oxide synthase with the postsynaptic density protein PSD-95 and alpha1-syntrophin mediated by PDZ domains. *Cell* **84**, 757–767.

Christopherson K. S., Hillier B. J., Lim W. A. and Bredt D. S. (1999) PSD-95 assembles a ternary complex with the *N*-methyl-D-aspartic acid receptor and a bivalent neuronal NO synthase PDZ domain. *J. Biol. Chem.* **274**, 27 467–27 473.

Davies E. V. and Hallett M. B. (1995) A soluble cellular factor directly stimulates $Ca^{2+}$ entry in neutrophils. *Biochem. Biophys. Res. Commun.* **206**, 348–354.

Doyle C., Holscher C., Rowan M. and Anwyl R. (1996) The selective neuronal NO synthase inhibitor 7-nitro-indazole blocks both long-term potentiation and depotentiation of field EPSPs in rat hippocampal CA1 in vivo. *J. Neurosci.* **16**, 418–424.

Endoh M., Maiese K. and Wagner J. A. (1994) Expression of the neural form of nitric oxide synthase by CA1 hippocampal neurons and other central nervous system neurons. *Neuroscience* **63**, 679–689.

Etter E. F., Minta A., Poenie M. and Fay F. S. (1996) Near-membrane [$Ca^{2+}$] transients resolved using the $Ca^{2+}$ indicator FFP18. *Proc. Natl Acad. Sci. USA* **93**, 5368–5373.

Garthwaite J., Charles S. L. and Chess-Williams R. (1988) Endothelium-derived relaxing factor release on activation of NMDA receptors suggests role as intercellular messenger in the brain. *Nature* **336**, 385–388.

Hawkins R. D., Son H. and Arancio O. (1998) Nitric oxide as a retrograde messenger during long-term potentiation in hippocampus. *Prog. Brain Res.* **118**, 155–172.

Iwase K., Iyama K., Akagi K., Yano S., Fukunaga K., Miyamoto E., Mori M. and Takiguchi M. (1998) Precise distribution of neuronal nitric oxide synthase mRNA in the rat brain revealed by non-radioisotopic in situ hybridization. *Brain Res. Mol. Brain Res.* **53**, 1–12.

Kiedrowski L., Costa E. and Wroblewski J. T. (1992) Glutamate receptor agonists stimulate nitric oxide synthase in primary cultures of cerebellar granule cells. *J. Neurochem.* **58**, 335–341.

Kojima H., Nakatsubo N., Kikuchi K., Kawahara S., Kirino Y., Nagoshi H., Hirata Y. and Nagano T. (1998) Detection and imaging of nitric oxide with novel fluorescent indicators: diaminofluoresceins. *Anal. Chem.* **70**, 2446–2453.

Kojima H., Urano Y., Kikuchi K., Higuchi T., Hirata Y. and Nagano T. (1999) Fluorescent indicators for imaging nitric oxide production. *Angew. Chem. Int. Ed. Engl.* **38**, 3209–3212.

Kornau H. C., Schenker L. T., Kennedy M. B. and Seeburg P. H. (1995) Domain interaction between NMDA receptor subunits and the postsynaptic density protein PSD-95. *Science* **269**, 1737–1740.

Marsault R., Murgia M., Pozzan T. and Rizzuto R. (1997) Domains of high $Ca^{2+}$ beneath the plasma membrane of living A7r5 cells. *EMBO J.* **16**, 1575–1581.

Miyawaki A., Griesbeck O., Heim R. and Tsien R. Y. (1999) Dynamic and quantitative $Ca^{2+}$ measurements using improved cameleons. *Proc. Natl Acad. Sci. USA* **96**, 2135–2140.

Niethammer M., Kim E. and Sheng M. (1996) Interaction between the C terminus of NMDA receptor subunits and multiple members of the PSD-95 family of membrane-associated guanylate kinases. *J. Neurosci.* **16**, 2157–2163.

Prast H. and Philippu A. (2001) Nitric oxide as modulator of neuronal function. *Prog. Neurobiol.* **64**, 51–68.

Sattler R., Xiong Z., Lu W. Y., Hafner M., MacDonald J. F. and Tymianski M. (1999) Specific coupling of NMDA receptor activation to nitric oxide neurotoxicity by PSD-95 protein. *Science* **284**, 1845–1848.

Son H., Hawkins R. D., Martin K., Kiebler M., Huang P. L., Fishman M. C. and Kandel E. R. (1996) Long-term potentiation is reduced in mice that are doubly mutant in endothelial and neuronal nitric oxide synthase. *Cell* **87**, 1015–1023.

Stuehr D. J. (1997) Structure–function aspects in the nitric oxide synthases. *Annu. Rev. Pharmacol. Toxicol.* **37**, 339–359.

Takata N., Shibuya K., Okabe M., Nagano T., Kojima H. and Kawato S. (2002) Pregnenolone sulfate acutely enhances NO production in the rat hippocampus: digital fluorescence study using NO reactive dye. *Bioimages* **10**, 1–8.

Takata N., Harada T., Rose J. A. and Kawato S. (2005) Spatiotemporal analysis of NO production upon NMDA and tetanic stimulation of the hippocampus. *Hippocampus* **15**, 427–440.

Uchino S., Kudo Y., Watanabe W., Nakajima-Iijima S. and Mishina M. (1997) Inducible expression of N-methyl-D-aspartate (NMDA) receptor channels from cloned cDNAs in CHO cells. *Brain Res. Mol. Brain Res.* **44**, 1–11.

Valtschanoff J. G. and Weinberg R. J. (2001) Laminar organization of the NMDA receptor complex within the postsynaptic density. *J. Neurosci.* **21**, 1211–1217.

Williams D. A. and Fay F. S. (1990) Intracellular calibration of the fluorescent calcium indicator Fura-2. *Cell Calcium* **11**, 75–83.

Williams D. A., Fogarty K. E., Tsien R. Y. and Fay F. S. (1985) Calcium gradients in single smooth muscle cells revealed by the digital imaging microscope using Fura-2. *Nature* **318**, 558–561.

Yun H. Y., Dawson V. L. and Dawson T. M. (1996) Neurobiology of nitric oxide. *Crit. Rev. Neurobiol.* **10**, 291–316.

 